論文 / 著書情報
Article / Book Information

Title	Heteroepitaxial spherical electroless Au-plated Pt-based nanogap electrodes of radius 5 nm and gap separation 0.7 nm
Authors	Yoon Young Choi, Ain Kwon, Yutaka Majima
Citation	Applied Physics Express, Volume 12, Number 12, 125003
Pub. date	2019, 11
Creative Commons	Information is in the article.

Applied Physics Express

Heteroepitaxial spherical electroless Au-plated Pt-based nanogap electrodes of radius 5 nm and gap separation 0.7 nm

OPEN ACCESS

Applied Physics Express 12, 125003 (2019)

LETTER

https://doi.org/10.7567/1882-0786/ab51df

Heteroepitaxial spherical electroless Au-plated Pt-based nanogap electrodes of radius 5 nm and gap separation 0.7 nm

Yoon Young Choi, Ain Kwon, and Yutaka Majima*

Laboratory for Materials and Structures, Institute of Innovative Research, Tokyo Institute of Technology, Yokohama 226-8503, Japan

*E-mail: majima@msl.titech.ac.jp

Received October 15, 2019; revised October 19, 2019; accepted October 28, 2019; published online November 14, 2019

Heteroepitaxial growth is demonstrated by electroless Au plating (ELGP) on polycrystalline Pt surface and initial ultrafine-linewidth Pt nanogap electrodes, confirmed by scanning transmission electron microscope cross-sectional images, atomic-resolution scanning electron microscope images, and energy-dispersive X-ray spectroscopy elemental maps. The gap between a pair of spherical multidomain heteroepitaxial Au on Pt electrodes of radius 5 nm is controlled to a value as small as 0.7 nm by the self-termination mechanism of ELGP without short circuit. The heteroepitaxial spherical Au/Pt nanogap electrodes are found to be robust against annealing at temperatures up to 573 K.

Supplementary material for this article is available online

Nanogap electrodes are the platforms for developing transistors on the scale of a few nm, such as a molecular transistor and a single-electron transistor (SET).[1–7] Owing to the development of semiconductor technologies guided by Moore's law, the gate length of transistors is as small as 10 nm, and will become a few nm within the next 10 years. It means that semiconductor technologies could soon start to access single functional π-conjugated molecules as semiconductor materials. The most commonly reported methods for the fabrication of nanogap electrodes include electromigration, electroplating, and oblique evaporation.[2–6] Molecular transistors have been prepared by introducing molecules into nanogap electrodes, and have been reported as SETs and Fowler-Nordheim transistors; however, measurement temperatures tend to be limited at low temperatures like 4 K.[8–14]

Our electroless Au plating (ELGP) is a unique method that enables the fabrication of multiple nanogaps simultaneously and to control the gap separation of nanogap electrodes.[15–18] We have developed a fabrication process for Au-based nanogap electrodes by combining ELGP with electron-beam lithography (EBL); the thus-obtained electrodes have a gap separation of 3.0 ± 1.7 nm, combined source-and-drain (S/D) linewidth of 90 nm, fabrication yield of 90%, and smooth surface with gap radius of 30 nm.[16–18] This high yield for narrowing the gap separation has been explained by a self-termination mechanism, in which mass transport of the plating Au ions in the nanogap region is restricted owing to a gap separation of only a few nm.[17] By using ELGP Au-based nanogap electrodes, we have demonstrated ideal SET logic operations[19–23] and molecular transport properties.[24] For obtaining larger gate capacitance for molecular transistors, we have tried to reduce the gap radii by narrowing the S/D linewidth of the electrodes to as small as 10 nm.[25] However, ultrafine Au-based nanogap electrodes with a 10 nm linewidth cannot be used for transistors owing to poor thermal stability attributed to Rayleigh instability.[25] We have changed the base electrode material from Au to Pt and have developed a process for the fabrication of robust ultra-fine Pt-based polycrystalline nanogap electrodes with 10 nm scale linewidth and 6 nm gap separation by using EBL.[25] However, to realize single-molecular transistors with high gate capacitance, an additional reduction in gap separation, to the same length of few-nm-scale single molecules, is required.

Herein we demonstrate heteroepitaxial Au growths by ELGP on polycrystalline Pt surface and initial ultrafine-linewidth Pt nanogap electrodes using scanning transmission electron microscope (STEM) cross-sectional images, atomic-resolution scanning electron microscope (SEM), and energy-dispersive X-ray spectroscopy elemental maps. The reduction in gap separation and radii of the Au gaps on Pt-based nanogap electrodes and their thermal stabilities are also demonstrated.

To fabricate ultrafine Pt-based nanogap electrodes, EBL processes were used in the manner described in our previous report.[25] Ultra-fine electrode patterns were drawn on an EBL resist-coated SiO_2/Si substrate by using an EBL apparatus (Elionix, ELS-7500EX). After EBL resist development, Ti and Pt were evaporated to obtain thicknesses of 3 nm and 10 nm, respectively, onto SiO_2/Si substrate via e-beam (EB) deposition. After a resist lift-off process, initial ultra-fine Pt-based nanogap electrodes were obtained.

ELGP process was performed on Pt electrodes and Pt-based nanogap electrodes in the manner described in our previous reports.[16,17] Briefly, for removing the organic contaminants or residual resist on Pt surface, initial ultra-fine Pt-based nanogap electrodes were cleaned by immersing in an acetone/ethanol mixture followed by UV-ozone cleaning. To prepare ELGP solution, Au sheet (99.99%, 65 mg) was dissolved in 3 ml of the commonly used medical iodine tincture (I_2 and KI in ethanol) with ultrasonic agitation and then, L(+)-ascorbic acid was added as a reducing agent in the Au-dissolved iodine tincture solution until saturation.[17] Finally, ELGP on the Pt surface was conducted by simply immersing cleaned Pt electrodes or initial Pt-based nanogap electrodes into the ELGP solution, which was diluted 1000 times by de-ionized water (8 ml, 18.1 MΩ). After immersion for the plating, the ELGP Pt electrodes and ELGP Pt-based nanogap electrodes were rinsed in de-ionized

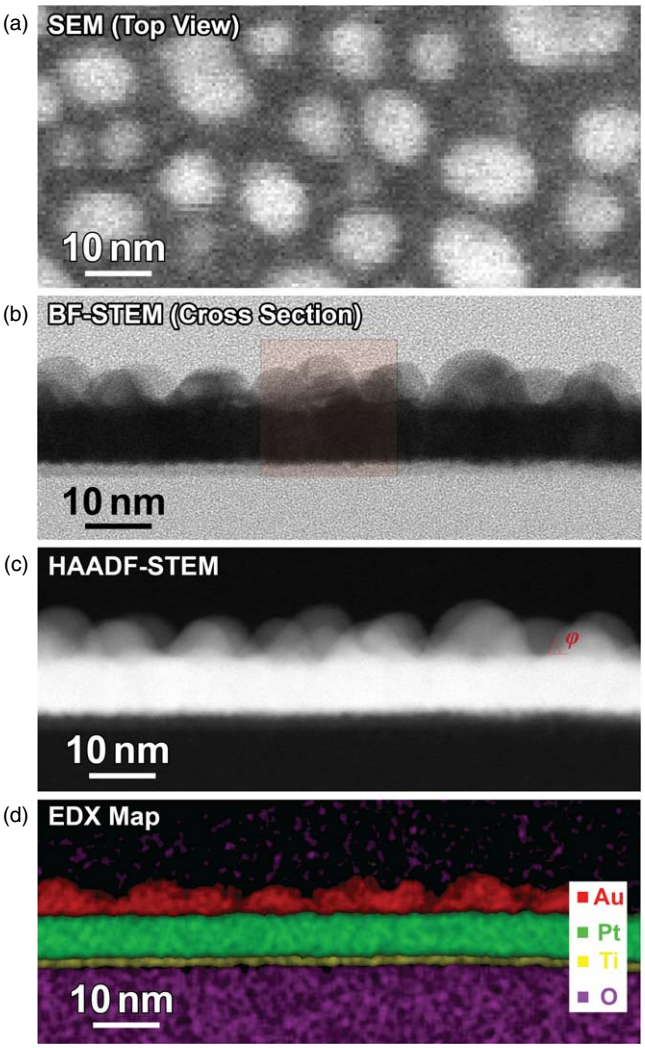

Fig. 1. (Color online) Scanning electron microscope (SEM) and scanning transmission electron microscope (STEM) images, and energy-dispersive X-ray spectroscopy (EDX) maps of the electroless Au-plated (ELGP) Pt-based electrode on SiO_2/Si substrate. (a) SEM image (top view), (b) bright-field (BF) STEM image (cross-section view), (c) high-angle annular dark-field (HAADF) STEM image, and (d) EDX elemental maps of Au, Pt, Ti, and O. (c) Contact angle (φ) of ELGP granular gold island (64°).

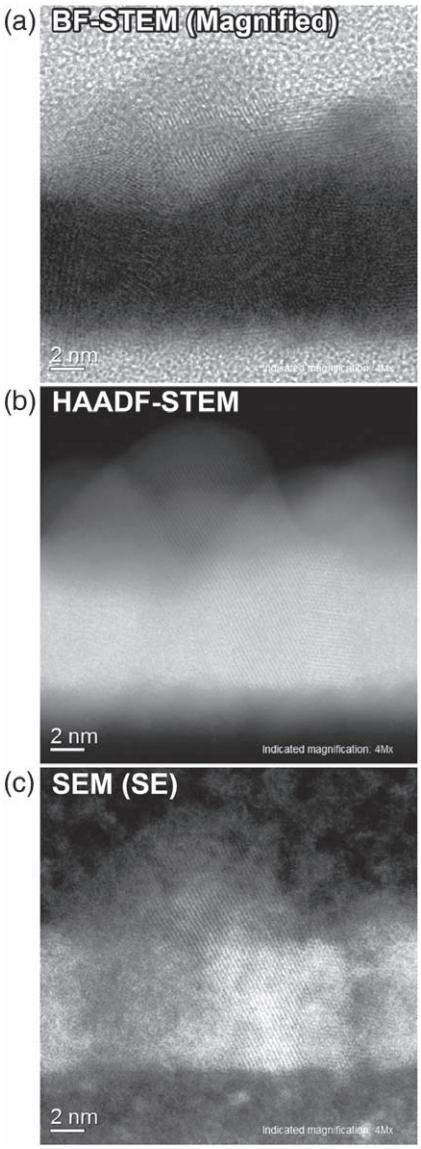

Fig. 2. Magnified cross-section images of the heteroepitaxial ELGP Pt-based electrode highlighted in Fig. 1(b) (red). (a) Spherical-aberration-corrected BF-STEM, (b) HAADF-STEM, and secondary-electron (SE) SEM images.

water and acetone/ethanol mixture for stopping Au plating. For confirming the thermal stability of the ELGP Pt-based nanogap electrodes, the nanogap electrodes were introduced in a vacuum furnace and were annealed for 2 h.

To observe top-view images of the ELGP Pt electrode and ELGP Pt-based nanogap electrodes, a field-emission scanning electron microscope (FE-SEM) (Hitachi, SU8000) was used. To prepare the thin samples for cross-section analysis of the studied electrodes, a focused ion beam SEM (FIB-SEM) (Hitachi, NX2000) was used. To observe and analyze the cross-section of ELGP Pt electrodes and ELGP Pt-based nanogap electrodes by SEM, STEM, and energy-dispersive X-ray spectroscopy (EDX) maps, a spherical-aberration-corrected STEM/SEM (Hitachi, HD-2700) was used. To observe the cross-section of ELGP Pt-based nanogap electrodes, FE-TEM (Hitachi, HF-3300) was used.

A top-view SEM image of ELGP on the flat surface of Pt-based nanogap electrodes [Fig. 1(a)] shows bright isolated granular structures. This SEM area was removed and sliced by FIB-SEM for cross-sectional analysis. The cross-sectional images obtained by bright-field (BF)-STEM, high-angle annular dark-field (HAADF)-STEM, and EDX elemental maps, are shown in Figs. 1(b)–1(d), respectively. The cross-sectional EDX elemental mapping shows Ti, Pt, and Au layers on SiO_2/Si substrate from the bottom to the top, without any alloying. The isolated granular structures are observed as overlapped hemispheric gold islands in the BF-STEM and HAADF-STEM images.

Notably, a typical contact angle of ELGP granular gold islands on the Pt surface is 64° as shown in Fig. 1(c), which are lower than 90°, suggesting that the chemical reduction rate of Au ions at the peripheral Pt surface of the granular gold island is almost same as that at the surface of the granular gold island. This large chemical reduction rate at the peripheral Pt surface leads the heteroepitaxial Au growth on Pt, since it generates Au-Pt bonds at the polycrystal Pt surface.

Magnified cross-sectional BF-STEM, HAADF-STEM, and secondary electron (SE)-SEM images of the ELGP granular gold islands on Pt layer, highlighted in Fig. 1(b) (red), are shown in Figs. 2(a)–2(c), respectively. The BF-STEM and

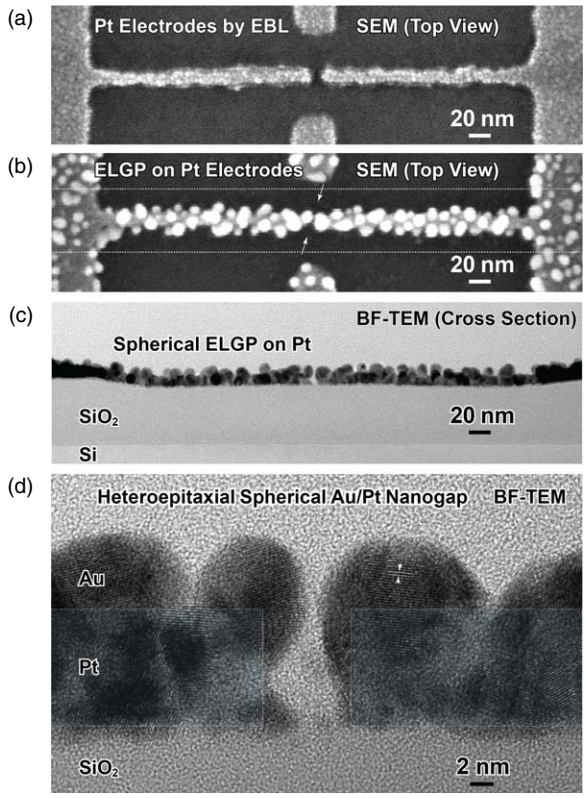

Fig. 3. (a) SEM image of ultrafine-linewidth Pt-based nanogap electrodes fabricated by electron beam lithography (EBL) on SiO_2/Si substrate. Heteroepitaxial spherical ELGP Pt-based nanogap electrodes. (b) SEM image (top view), (c) BF-TEM image (cross-section view), and (d) magnified BF-TEM. In Fig. 3(d), Pt nanogap is highlighted in blue. Lattice fringes has a lattice parameter of 2.31 Å (a pair of parallel lines with arrows), indicating heteroepitaxial Au (111) growth on polycrystalline Pt (111) by ELGP.

HAADF-STEM images show lattice fringes of the Pt(111) planes as different parallel lines with equal spacing in the middle dark and bright layers, respectively. The EDX elemental map in Fig. 1(d) shows that this middle layer is Pt. Therefore, the EB-evaporated Pt layer is polycrystalline in nature. On the polycrystalline Pt layer, isolated hemispheric Au islands are observed in the overlapped BF-STEM and HAADF-STEM images. Every hemispheric Au island tends to have unique parallel lines as shown in the BF-STEM image [Fig. 2(a)]. At the cross-sectional surface observed by SE-SEM, the lattice fringe of Pt(111) is connected to that of ELGP Au(111), which is sufficient evidence of the heteroepitaxial growth of Au on polycrystalline Pt by ELGP. This evidence is also supported by the BF-STEM and HAADF-STEM images [Figs. 2(a) and 2(b), respectively].

Heteroepitaxial growths of Au on a single-crystal Pt(111) surface by electrodeposition and evaporation by Knudsen cell in ultrahigh vacuum have been widely reported.[26–29] However, to the best of our knowledge, heteroepitaxial growth of electroless plated Au on polycrystalline Pt surface has not been reported. In this study, Pt surface was prepared by usual EB-deposition.

The SEM image of typical ultrafine Pt-based nanogap electrodes with two side-gate electrodes fabricated by EBL is shown in Fig. 3(a). The Pt-based nanogap electrodes have gap separation and S/D linewidths of 7 and 11 nm, respectively, the same as those mentioned in the previous report.[25] These values of gap separation and S/D linewidths are already almost on the sub-10 nm scale. However, additional decrease in gap separation to single molecular length is required for single-molecular transistors. Therefore, ELGP was used for the synthesis of ultrafine Pt-based nanogap electrodes.

The top-view SEM image of Pt-based nanogap electrodes after ELGP is shown in Fig. 3(b). Bright isolated granular structures were observed, similar to what was observed in the case of ELGP on the surface of the polycrystalline Pt-based nanogap electrodes. These ultrafine ELGP Pt-based nanogap electrodes show a pair of unique spherical structures in the gap with a top radius of 5 nm.

The two side-gate electrodes of the ELGP Pt-based nanogap electrodes were removed and sliced from both sides up to the dotted lines observed in FIB-SEM images. The cross-sectional BF-STEM image [Fig. 3(c)] shows the spherical Au structure produced by ELGP, and every sphere in the BF-STEM image corresponds to those in the SEM image shown in Fig. 3(b). The Au spheres grow at not only the top but also a side of the Pt-nanorod structure, owing to the almost square rod cross-section with Pt-thickness and linewidth of 10 and 11 nm, respectively.

Magnified cross-sectional BF-TEM image of the ELGP Pt-based nanogap electrodes [Fig. 3(c)] is shown in Fig. 3(d), taken from the direction of the pair of arrows shown in Fig. 3(b). Certain cross-sectional areas of the Pt electrodes are highlighted as two blue rectangles in Fig. 3(d). Notably, the nanogap consists of a pair of polycrystalline spherical shapes with radii of 2.8 (left) and 4.3 (right) nm to minimize the surface energy for a given volume. Since Pt electrodes are involved within the spheres, multidomain heteroepitaxial Au growth on Pt by ELGP has also been observed.

The gap separation was determined from the cross-sectional profiles of the heteroepitaxial spherical Au/Pt nanogap in the BF-TEM images. The gap separation was evaluated to be 0.35 nm and 0.70 nm in directions perpendicular to the nanorods and where the evaluated gap separation was the largest, respectively, as shown in Fig. S1(b) and S1(c) in the supplementary information, available online at stacks.iop.org/APEX/12/125003/mmedia. Consequently, the accurate gap separation was decided as 0.70 nm.

This extraordinarily small gap separation of 0.70 nm exists between two multidomain heteroepitaxial Au/Pt spheres with radii of 2.8 and 4.3 nm. Self-termination of ELGP reportedly restricts the growth of the electroless Au plating owing to the mass transport of the plating Au ions at the gap.[16,17] The gap separation and the radius of the ELGP Au-based (Au/Au) nanogap electrodes were previously reported to be 3.0 and 45 nm, respectively; the corresponding values of 0.7 nm and 4.3 for the heteroepitaxial spherical Au/Pt nanogap electrodes are ~4 and 10 times smaller, apparently improving the gate capacitance of nanogap-based transistors. The current between the 0.7 nm nanogap electrodes was less than 10 pA under the bias voltage application of 0.1 V through the electrode pads. As the gap separation has been controlled as small as 3 atomic scales without short circuit, the plating Au ion was reduced one by one, and diffused at the surfaces of the pair of the heteroepitaxial Au/Pt spheres during the ELGP process to minimize the surface energy for a given volume. Since the radii of the Au/Pt pair spheres are as small as a few nm, the plating Au ions could approach close to the

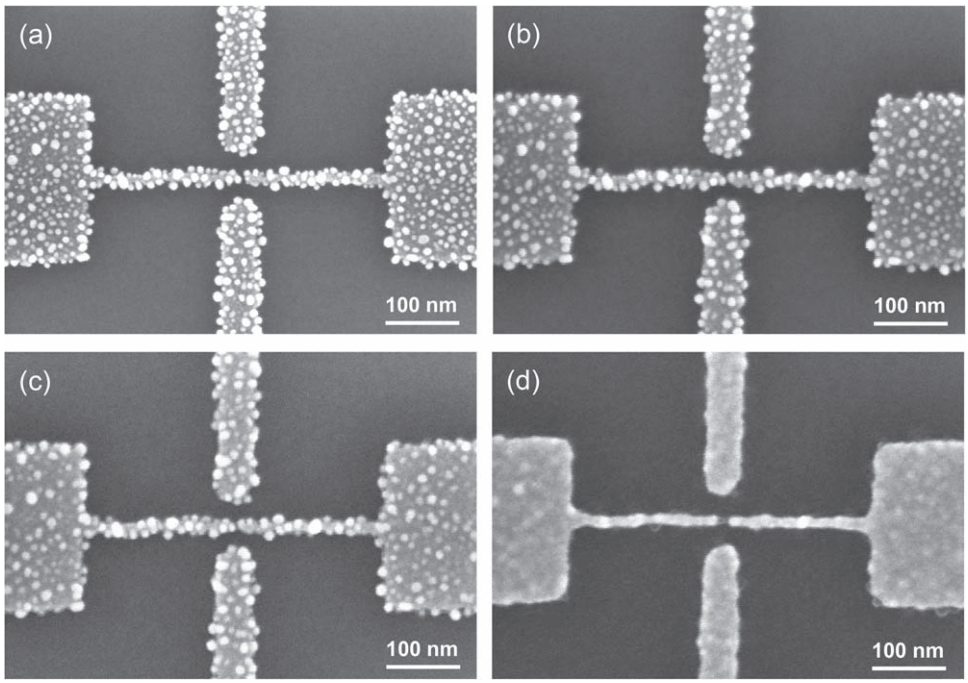

Fig. 4. SEM images of heteroepitaxial spherical ELGP Pt-based nanogap electrodes (a) before annealing and after annealing at (b) 473 K, (c) 573 K, and (d) 673 K in a vacuum furnace.

gap region compared with the previous Au/Au pair spheres with 45 nm in radii.[16,17] Consequently, the extraordinary small gap formation of 0.7 nm has been obtained by the self-termination mechanism under the ultra-small radii of Au/Pt spheres with a few nm.

From the lattice fringes shown in Fig. 3(d), the heteroepitaxial spherical Au growth on Pt nanogap ends is confirmed. The distance between a pair of parallel lines [highlighted in Fig. 3(d)] is calculated to be 2.31 Å, almost equal to the lattice plane distance of Au(111) (2.35 Å).

The continuous crystal growth of Au (111) along the Pt (111) plane has been reported for Au evaporation and Au electrodeposition on the highly cleaned Pt (111) single crystal.[26–29] Krupski et al. demonstrated that the perfectly wetted Au crystal can grow on Pt single crystal because Au has lower surface energy than and almost the same lattice constant as Pt.[26] Practically, the surface free energy of the Pt (111) surface ($2.299\,\mathrm{J\,m^{-2}} < \Upsilon < 2.489\,\mathrm{J\,m^{-2}}$) is higher than that of the Au (111) surface ($1.283\,\mathrm{J\,m^{-2}} < \Upsilon < 1.506\,\mathrm{J\,m^{-2}}$).[26,30] Therefore, this heteroepitaxial spherical Au (111) growth along the polycrystalline Pt (111) during ELGP is supported by the surface free energy. However, this multidomain heteroepitaxial Au growth along the polycrystalline Pt is observed not upon ultrahigh vacuum evaporation or electrodeposition, but by using an ELGP process.

The thermal stability of heteroepitaxial spherical Au/Pt nanogap electrodes are analyzed as shown in the SEM images obtained after annealing [Figs. 4(a)–4(d)]. The heteroepitaxial spherical Au/Pt nanogap electrodes did not show any changes in their structure after annealing at 473 K for 2 h [Fig. 4(b)]. Upon increasing the annealing temperature to 573 K for 2 h [Fig. 4(c)], the heteroepitaxial spherical Au/Pt nanogap electrodes maintained the unique structure with the same gap separation, although some of the spherical Au structures on the flat Pt electrodes began to diffuse on the Pt surface due to Rayleigh instability. After annealing at 673 K for 2 h [Fig. 4(d)], the heteroepitaxial spherical Au structures on Pt-based nanogap electrodes disappeared and were completely diffused on the Pt surface. Consequently, the thermal stability of the heteroepitaxial spherical Au/Pt nanogap electrodes at temperatures up to 573 K was higher than the previously reported Au/Au nanogap electrodes with ~90 nm scale S/D linewidth, which was deformed into droplets at 573 K owing to Rayleigh instability.[25]

Based on the SEM images shown in Figs. 1(a) and 2(b), the heteroepitaxial Au spheres grown by ELGP on polycrystalline Pt tend to be isolated from the next Au spheres. Since the surface diffusion coefficient of Au is 10^7–10^8 times higher than that of Pt, Au atoms tend to diffuse even at room temperature if the gap radius is smaller than 5 nm.[25,31] This is because the surface tension is inversely proportional to the radius of the spherical structure. Consequently, the Au–Pt bond at the heteroepitaxial interface restricts Au atom diffusion at the Pt surface despite the extremely large surface tension. This robustness of the spherical Au structure on polycrystalline Pt surface after annealing is remarkable if we consider the small radius of 5 nm.

In conclusion, heteroepitaxial Au growth has been demonstrated on Pt by using ELGP. Multidomain heteroepitaxial Au spheres of radius 5 nm were observed in Pt-based nanogap electrodes. Owing to the self-termination mechanism, the gap separation was controlled to a value as small as 0.7 nm without short circuit. The heteroepitaxial spherical Au/Pt nanogap was more robust against annealing up to 573 K than the Au/Au nanogap because of heteroepitaxial growth. The small radius and the robustness of the heteroepitaxial spherical Au/Pt nanogap electrodes encourage the development of few-nm-scale molecular transistors with gate capacitance large enough to operate at room temperature.

Acknowledgments We thank Ms. M. Miyakawa for technical support regarding SEM. We thank Mr. T. Okubo and Mr. T. Sato, Hitachi High-Technologies for technical support regarding FIB-SEM, TEM, and STEM/SEM. This study was partially supported by the MEXT Elements Strategy Initiative to Form Core Research Centers, Tokyo Institute of Technology, and BK Plus Program, the Basic Science Research Program (NRF-2014R1A6A1030419).

ORCID iDs Yutaka Majima https://orcid.org/0000-0002-5108-1934

1) N. D. Lang and P. M. Solomon, IEEE Trans. Nanotechnol. **14**, 918 (2015).
2) T. Li, W. Hu, and D. Zhu, Adv. Mater. **22**, 286 (2010).
3) H. Song, M. A. Reed, and T. Lee, Adv. Mater. **23**, 01583 (2011).
4) D. Xiang, X. Wang, C. Jia, T. Lee, and X. Guo, Chem. Rev. **116**, 4318 (2016).
5) Y. Naitoh, Q. Wei, M. Mukaida, and T. Ishida, Appl. Phys. Express **9**, 035201 (2016).
6) Y. Yang, C. Gu, and J. Li, Small **15**, 1804177 (2019).
7) K. K. Likharev, Proc. IEEE. Mater. **87**, 606 (1999).
8) A. Aviram and M. A. Ratner, Chem. Phys. Lett. **29**, 277 (1974).
9) M. A. Reed, C. Zhou, C. J. Muller, T. P. Burgin, and J. M. Tour, Science **278**, 252 (1997).
10) H. Park, J. Park, A. K. L. Lim, E. H. Anderson, A. P. Alivisatos, and P. L. McEuen, Nature **407**, 57 (2000).
11) S. Kubatkin, A. Danilov, M. Hjort, J. Cornil, J. L. Bredas, N. Stuhr-Hansen, P. Hedegard, and T. Bjornholm, Nature **425**, 698 (2003).
12) A. N. Pasupathy, R. C. Bialczak, J. Martinek, J. E. Grose, L. A. K. Donev, P. L. McEuen, and D. C. Ralph, Science **306**, 86 (2004).
13) H. Song, Y. Kim, Y. H. Jang, H. Jeong, M. A. Reed, and T. Lee, Nature **462**, 1039 (2009).
14) L. Sun, Y. A. Daiz-Fernandez, T. A. Gschneidtner, F. Westerlund, S. Lara-Avila, and K. Moth-Poulsen, Chem. Soc. Rev. **43**, 7378 (2014).
15) C. S. Ah, Y. J. Yun, J. S. Lee, H. J. Park, D. H. Ha, and W. S. Yun, Appl. Phys. Lett. **88**, 133116 (2006).
16) Y. Yasutake, K. Kono, M. Kanehara, T. Teranishi, M. R. Buitelaar, C. G. Smith, and Y. Majima, Appl. Phys. Lett. **91**, 203107 (2007).
17) V. M. V. Serdio, Y. Azuma, S. Takeshita, T. Muraki, T. Teranishi, and Y. Majima, Nanoscale **4**, 7161 (2012).
18) V. M. V. Serdio, T. Muraki, S. Takeshita, D. E. S. Hurtado, S. Kano, T. Teranishi, and Y. Majima, RCS Adv. **5**, 22160 (2015).
19) Y. Azuma, Y. Yasutake, K. Kono, M. Kanehara, T. Teranishi, and Y. Majima, Jpn. J. Appl. Phys. **49**, 090206 (2010).
20) K. Maeda, N. Okabayashi, S. Kano, S. Takeshita, D. Tanaka, M. Sakamoto, T. Teranishi, and Y. Majima, ACS Nano **6**, 2798 (2012).
21) S. Kano, Y. Azuma, K. Maeda, D. Tanaka, M. Sakamoto, T. Teranishi, L. W. Smith, C. G. Smith, and Y. Majima, ACS Nano **6**, 9972 (2012).
22) S. Kano, D. Tanaka, M. Sakamoto, T. Teranishi, and Y. Majima, Nanotechnol. **26**, 045702 (2015).
23) Y. Majima, G. Hackenberger, Y. Azuma, S. Kano, K. Matsuzaki, T. Susaki, M. Sakamoto, and T. Teranishi, Sci. Tech. Adv. Mater. **18**, 374 (2017).
24) C. Ouyang, K. Hashimoto, H. Tsuji, E. Nakamura, and Y. Majima, ACS Omega **3**, 5125 (2018).
25) Y. Y. Choi, T. Teranishi, and Y. Majima, Appl. Phys. Express **12**, 025002 (2019).
26) K. Krupski, M. Moors, P. Jozwik, T. Kobiela, and A. Krupski, Materials **8**, 2935 (2015).
27) F. Sibert, F. Ozanam, F. Maroun, R. J. Behm, and O. M. Magnussen, Surf. Sci. **572**, 115 (2004).
28) S. Ambrozik, C. Mitchell, and N. Dimitrov, J. Electrochem. Soc. **163**, D3001 (2016).
29) Y.-C. Yang, S.-L. Yau, and Y.-L. Lee, J. Am. Chem. Soc. **128**, 3677 (2006).
30) L. Vitos, A. V. Ruban, H. L. Skriver, and J. Kollar, Surf. Sci. **411**, 186 (1998).
31) C. Alonso, R. C. Salvarezza, J. M. Vara, A. J. Arvia, L. Vazquenz, A. Bartolome, and A. M. Baro, J. Electrochem. Soc. **137**, 2161 (1990).